

Effects of Al doping on the structural and electronic properties of $Mg_{1-x}Al_xB_2$

O. de la Peña, A. Aguayo, and R. de Coss

Departamento de Física Aplicada, Centro de Investigación y de Estudios Avanzados
Apartado Postal 73 Cordemex 97310 Mérida, Yucatán, México
(December 27, 2021)

We have studied the structural and electronic properties of $Mg_{1-x}Al_xB_2$ within the Virtual Crystal Approximation (VCA) by means of first-principles total-energy calculations. Results for the lattice parameters, the electronic band structure, and the Fermi surface as a function of Al doping for $0 \leq x \leq 0.6$ are presented. The ab initio VCA calculations are in excellent agreement with the experimentally observed change in the lattice parameters of Al doped MgB_2 . The calculations show that the Fermi surface associated with holes at the boron planes collapses gradually with aluminum doping and vanishes for $x = 0.56$. In addition, an abrupt topological change in the π -band Fermi surface was found for $x = 0.3$. The calculated hole density correlates closely with existing experimental data for $T_c(x)$, indicating that the observed loss of superconductivity in $Mg_{1-x}Al_xB_2$ is a result of hole band filling.

PACS: 74.25.Jb, 74.62.Dh, 74.70.Ad, 74.70.Dd

The discovery of superconductivity in the simple binary intermetallic compound MgB_2 with a T_c as high as $40 K$ has stimulated intense investigations, both from the experimental and the theoretical points of view². The superconducting transition temperature T_c for MgB_2 has been studied as a function of pressure and alloying². Pressure studies have shown that T_c decreases with applied hydrostatic pressure^{3,5}, which has been explained by an increase of the band filling of the boron bands with pressure^{4,5}. Thus, the change in the band filling in MgB_2 under pressure is an effect of the reduction of the cell volume with pressure^{4,5}.

Experimentally it has been observed that the superconducting transition temperature of $Mg_{1-x}Al_xB_2$ decrease with Al doping^{6,7}, and superconductivity disappears for $x > 0.58$ ⁹. According to band structure calculations of MgB_2 , electron doping reduces the density of states (DOS) at the Fermi level^{10,11}. Based on the Rigid Band Approximation, An and Pickett¹⁰ analyzed the effect of Al doping on the DOS of MgB_2 , and found that the DOS at the Fermi level drops for $x \geq 0.25$. Structural characterization of $Mg_{1-x}Al_xB_2$ shows that the cell volume also decreases with Al doping^{6,7}. Therefore, the band filling in $Mg_{1-x}Al_xB_2$ is expected to have two contributions: the first is due to the electron doping, and the second is a result of the cell volume reduction as in the case of pressure effects.

Measurements of the thermoelectric power, S , on $Mg_{1-x}Al_xB_2$ for $x \leq 0.1$ have shown that the slope of the linear part of $S(T)$ changes with Al doping, indicating changes in the Fermi surface due to electron doping¹². More recently, it was shown that the Raman spectra of $Mg_{1-x}Al_xB_2$ for $0 \leq x \leq 0.6$ ^{8,9} show a pronounced frequency shift and a considerable change in the line-width for the E_{2g} phonon mode at $x = 0.3$, which correlate with a steeping in the behavior of $T_c(x)$ with Al doping^{6,8,9}. Although some of the observed effects of Al doping in $Mg_{1-x}Al_xB_2$ can be interpreted qualitatively in terms

of the Rigid Band Approximation as an effect of the band filling, a quantitative analysis is essential in order to determine the interplay between electron doping and the structural, electronic, and transport properties of $Mg_{1-x}Al_xB_2$.

In this paper, we present a study of the effects of Al doping on the structural and electronic properties of $Mg_{1-x}Al_xB_2$ for $0 \leq x \leq 0.6$, using the ab initio Virtual Crystal Approximation. The calculated lattice parameters are compared with available experimental data⁶. The evolution of the electronic band structure and the π -band Fermi surface (FS) as a function of Al doping is analyzed. We correlate our results to the experimentally observed behavior of T_c with Al doping^{6,9}. We show that the observed loss of superconductivity in $Mg_{1-x}Al_xB_2$ can be explained by the filling of the hole bands.

The Kohn-Sham total energies were calculated self-consistently using the full-potential linearized augmented plane-wave method (LAPW)¹³ as implemented in the WIEN 97 code¹⁴, where the core states are treated fully relativistically, and the semicore and valence states are computed in a scalar relativistic approximation. The exchange correlation potential was evaluated within the generalized gradient approximation (GGA), using the recent parameter-free GGA form by Perdew, Burke, and Ernzerhof¹⁵. We chose muffin-tin radii (R_{MT}) of 1.8 and 1.5 a.u. for Mg and B, respectively, and used a plane-wave cutoff $R_{MT}K_{MAX} = 9.0$. Inside the atomic spheres the potential and charge density were expanded in crystal harmonics up to $l = 10$. Convergence was assumed when the energy difference between the input and output charge densities was less than $1 \cdot 10^{-5}$ Ryd. Special attention was paid to convergence of results by performing the calculations for a sufficiently large number of k points in the irreducible wedge of the Brillouin zone for the omega structure (144 k points). The corrected tetrahedron method was used for Brillouin-zone integration¹⁶.

The Al doping was modeled in the ab initio Virtual

Crystal Approximation (VCA)^{17;18}. The Mg ($Z = 12$) sites are substituted by pseudo-atoms which have a fractional electronic charge ($Z = 12 + x$), depending on the Al concentration, x . This approximation is justified mainly by the fact that Al only has one electron more than Mg. The full-potential for the VCA system is determined self-consistently for each value of Al doping without shape approximation¹⁴. The *ab initio* VCA as implemented in this work has been used very recently to model Cu and Be substitutions in MgB₂¹⁸. The equilibrium lattice parameters were determined by total-energy calculations for each value of Al doping ($x = 0.0, 0.1, 0.2, 0.25, 0.3, 0.35, 0.4, 0.5$, and 0.6). Since the AB₂ (omega) structure has two structural parameters (a and c), we performed self-consistent total-energy calculations for nine different volumes and for nine different c/a ratios, in order to optimize both V and c/a for each Al concentration. For MgB₂ we have obtained $a = 3.083$ Å and $c = 3.526$ Å, which compares very well to the experimental values of $a = 3.086$ Å and $c = 3.524$ Å¹, respectively.

In Fig. 1 we present the calculated lattice parameters (a and c) of Mg_{1-x}Al_xB₂ for $0 \leq x \leq 0.6$, and it can be seen that both a and c decrease with Al doping as observed experimentally^{6;7}. For comparison we have included the experimental data from Slusky et al.⁶, and we find that the change in a with Al doping is very well reproduced by the VCA calculations. For the region $0.1 \leq x \leq 0.2$ two values of c were reported⁶, which has been ascribed to the coexistence of two phases (Mg-rich and Al-rich phases). It is interesting to note that in this region the VCA values approximately reproduce the average value. However, for $x > 0.2$ we find very good agreement between the experimental data and the VCA calculations (see Fig. 1). Although both cell parameters (a and c) decrease monotonically with Al doping, it is interesting to note that the slope for c as a function of Al doping is larger than for a . In order to understand this behavior in the context of bonding properties we have analyzed the change in the charge distribution with Al doping. Fig. 2(a) shows the charge density distribution in the (110) plane of MgB₂. Mg nuclei are located at the corners of the map and B nuclei are at the (1=3;1=2) and (2=3;1=2) positions, all of them in the plane of the figure. We can see the directional, covalent B-B bonds. In addition, there is a significant density of charge in the interstitial region giving rise to metallic-type bonding between the Mg and B planes. The charge distribution and bonding properties of MgB₂ have been calculated previously and were discussed in detail in Ref. 19. Therefore, we concentrate on the influence of Al doping on the electron density of MgB₂. Fig. 2(b) shows the difference between the charge densities of Mg_{0.5}Al_{0.5}B₂ and MgB₂. It can be seen that charge transfer occurs from Al-B ions into the nearby interstitial region. We can see that the majority of this charge is distributed in the inter-plane region, and an important fraction of the charge is being transferred to the σ -bond, while only a small fraction is at

the π -bond in the boron planes. This important increase in occupation of the σ -bond with Al doping accounts for the strong decrease of the separation between planes (the c axis) of Mg_{1-x}Al_xB₂.

The evolution of the calculated DOS for Mg_{1-x}Al_xB₂, not shown here, shows a band broadening as a function of Al doping, mainly as a consequence of the cell volume reduction. In addition, electron doping raises the Fermi level to higher energies. Both effects, band broadening and electron doping, contribute to reduce the density of states at the Fermi level in Al-doped MgB₂. In Table I, we summarize the calculated lattice parameters, cell volume, and the total density of states at the Fermi level $N(E_F)$ for each of the studied Al concentrations. We can see that $N(E_F)$ decreases with Al doping, from 0.72 for MgB₂ to 0.26 states/eV per cell for Mg_{0.4}Al_{0.6}B₂. Therefore, in a BCS scenario this reduction in $N(E_F)$ accounts for the decrease of T_C with Al doping in Mg_{1-x}Al_xB₂^{6;9}.

A careful analysis of the x -dependence of the electronic band structure, and in particular of the σ -band FS which has been shown to be relevant for superconductivity in MgB₂^{10;11;20;23}, provides a more detailed and quantitative description of the effects of Al doping. In Fig. 3 we present the electronic band structure of MgB₂. The σ -bands coming from the sp boron orbitals, are strongly two-dimensional with very little dispersion along Γ -A, this dispersion can be characterized by the difference between the E_{Γ} and E_A energies (see Fig. 3). The E_{Γ} and E_A energies correspond to the bottom and top of the σ -band in the Γ -A direction, respectively. The light-hole and heavy-hole π -bands in MgB₂ form a FS consisting of two nested cylinders surrounding the Γ -A line in the Brillouin zone (see Fig. 3). The dependence of the energy of the σ -bands at Γ and A relative to E_F as a function of Al doping are shown in Fig. 4. We can see that both energies, E_{Γ} and E_A , decrease monotonically as a function of Al doping. More interestingly, the Fermi level reaches E_{Γ} for $x = 0.3$ and E_A for $x = 0.56$. We find that the radius of the cylinders decreases gradually with Al doping and at a critical concentration of $x = 0.3$, the radius at $k_z = 0$ collapses and the FS takes the form of a sandglass. A three-dimensional view of the changes in the FS topology with Al doping are presented in Fig. 4. For $x = 0.3$ the Fermi level in σ is at a saddle point in the band structure, and the transition through the saddle point results in the disruption of the neck, i.e., the transition from a closed to an open section of FS²⁴. For $x > 0.3$ the FS takes the form of two cones (see Fig. 4), and these finally vanishes at the second critical concentration ($x = 0.56$) when the hole bands have been filled. These changes in the hole FS are expected to be accompanied by various kinds of electronically driven anomalies, including lattice dynamics and transport properties.

As was mentioned above, Raman spectroscopy studies on Mg_{1-x}Al_xB₂^{8;9} show a pronounced shift and a considerable change in the line-width of the E_{2g} phonon mode at $x = 0.3$. Additionally, a steeping of the T_C decrease has

been observed at an Al concentration of approximately 0.3^{6,8,9}. These changes in both the structural and the superconducting properties seem to be strongly related to the abrupt change in the FS topology, which occurs for $x = 0.3$ (see Fig. 4). In order to establish a more direct comparison between the FS evolution and the superconducting properties with increasing the Al doping, we have calculated the hole FS area as a function of x , which is proportional to the hole density at the Fermi level. In Fig. 4(b) we compare the calculated normalized FS area, $A_{FS}(x) = A_{FS}(0)$, with the normalized superconducting critical temperature, $T_c(x) = T_c(0)$. The experimental data for $T_c(x)$ were taken from Ref. 8. We can see that for the low concentration region ($x < 0.25$), before the E_{2g} phonon frequency shift⁹, the drop of T_c is directly related to the change in the hole density. This view is in agreement with recent results of NMR experiments on Al-doped MgB_2 for $x < 0.1$ ²⁵. In the high concentration region ($x > 0.25$), the behavior of T_c is determined by the FS area but the importance of the phonon-renormalization is clear^{8,9}. In this way, the FS area and T_c follow the same behavior with Al doping in the whole range ($0 < x < 0.6$), indicating a close relation between the changes in the γ -band FS and the loss of superconductivity in Al-doped MgB_2 .

In summary, we have performed a first-principles study of the effects of Al doping on the structural parameters, the electronic structure, and the γ -band FS of $Mg_{1-x}Al_xB_2$, using the Virtual Crystal Approximation. (i) We find that the ab initio VCA calculations are in excellent agreement with the experimentally observed changes in the lattice parameters as a function of Al doping. (ii) The analysis of the charge density shows that an important portion of the Al-electrons are at the inter-plane region and only a small fraction at the B-B planes, providing an explanation for the strong change of the c -axis and the small change in the a -axis with the Al concentration. (iii) The hole FS gradually collapses with Al doping and vanishes for $x = 0.56$. An abrupt topological change was found for $x = 0.3$, which correlates with the frequency shift of the E_{2g} phonon mode and the steeping in the $T_c(x)$ decrease. Additionally, the critical concentration of $x = 0.56$ at which the hole FS disappears, corresponds to the experimentally observed Al concentration (0.5-0.6) for which $T_c(x)$ vanishes. (iv) We find that the behavior of the calculated γ -band FS area with Al doping correlates with the superconducting critical temperature $T_c(x)$. Consequently, the observed loss of superconductivity in $Mg_{1-x}Al_xB_2$, can be explained as a result of the filling of the hole bands.

This research was funded by the Consejo Nacional de Ciencia y Tecnología (CONACYT, México) under Grant No. 34501-E. Two of the authors (O.P. and A.A.) gratefully acknowledge a student fellowship from CONACYT-México. The authors would like to thank Dimitris Papaconstantopoulos and David Singh for valuable discussions.

Author to whom correspondence should be addressed. Electronic address: decoss@mda.cinvestav.mx

- ¹ J. Nagamatsu, N. Nakagawa, T. Muranaka, Y. Zenitai, and J. Akimitsu, *Nature* **410**, 63 (2001).
- ² C. Buzea and T. Yamashita, *Supercond. Sci. Technol.* **14**, R115 (2001).
- ³ M. M. Onteverde, M. Nunez-Regueiro, N. Rogado, K. A. Regan, M. A. Hayward, T. He, S. M. Loureiro, and R. J. Cava, *Science* **292**, 75 (2001).
- ⁴ K. Prassides, Y. Iwasa, T. Ito, D. H. Chi, K. Uehara, E. Nishibori, M. Takata, M. Sakata, Y. Ohishi, O. Shimomura, T. Muranaka, and J. Akimitsu, *Phys. Rev. B* **64**, 012509 (2001).
- ⁵ P. Bordet, M. Mezouar, M. Nunez-Regueiro, M. M. Onteverde, M. D. Nunez-Regueiro, N. Rogado, K. A. Regan, M. A. Hayward, T. He, S. M. Loureiro, and R. J. Cava, *Phys. Rev. B* **64**, 172502 (2001).
- ⁶ J. S. Slusky, N. Rogado, K. A. Regan, M. A. Hayward, P. Khalifah, T. He, K. Inumaru, S. M. Loureiro, M. K. Hass, H. W. Zandbergen, and R. J. Cava, *Nature* **410**, 343 (2001).
- ⁷ A. Bianconi, D. Di Castro, S. Agrestini, G. Campi, N. L. Saini, A. Saccone, S. De Negri, and M. Giovannini, *J. Phys.: Condens. Matter* **13**, 7383 (2001).
- ⁸ P. Postorino, A. Congeduti, P. Dore, A. Nucara, A. Bianconi, D. Di Castro, S. De Negri, and A. Saccone, *Phys. Rev. B* **65**, 020507 (2002).
- ⁹ B. Renker, K. B. Bohnen, R. Heid, D. Ernst, H. Schober, M. Koza, P. Adelmann, P. Schweiss, and T. Wolf, *Phys. Rev. Lett.* **88**, 067001 (2002).
- ¹⁰ J. M. An and W. E. Pickett, *Phys. Rev. Lett.* **86**, 4366 (2001).
- ¹¹ J. Kortus, I. I. Mazin, K. D. Belashchenko, V. P. Antropov, and L. L. Boyer, *Phys. Rev. Lett.* **86**, 4656 (2001).
- ¹² B. Lorenz, R. L. Meng, Y. Y. Xue, and C. W. Chu, *Phys. Rev. B* **64**, 052513 (2001).
- ¹³ D. J. Singh, *Plane Waves, Pseudopotentials and the LAPW Method* (Kluwer Academic Publishers, Boston, 1994).
- ¹⁴ P. Blaha, K. Schwarz, and J. Luitz, computer code WIEN 97 (Vienna University of Technology, 1997), improved and updated Unix version of the original copyrighted WIEN code, which was published by P. Blaha, K. Schwarz, P. Sorantin, and S. B. Trickey, *Comput. Phys. Commun.* **59**, 339 (1990).
- ¹⁵ J. P. Perdew, S. Burke, and M. Ernzerhof, *Phys. Rev. Lett.* **77**, 3865 (1996).
- ¹⁶ P. E. Blöchl, O. Jepsen, and O. K. Andersen, *Phys. Rev. B* **49**, 16223 (1994).
- ¹⁷ D. A. Papaconstantopoulos, E. N. Economou, B. M. Klein, and L. L. Boyer, *Phys. Rev. B* **20**, 177 (1979).
- ¹⁸ M. J. Mehl, D. A. Papaconstantopoulos, and D. J. Singh, *Phys. Rev. B* **64**, (2001).
- ¹⁹ K. D. Belashchenko, M. van Schilfegaarde, V. P. Antropov, *Phys. Rev. B* **64**, 092503 (2001); P. Ravindran, P. Vajeston, R. Vijiya, A. K. Jekshus, and H. Fjellvåg, *Phys. Rev. B* **64**, 224509 (2001).

- ²⁰ Y. Kong, O.V. Dolgov, O. Jepsen, and O.K. Andersen, Phys. Rev. B 64, 020501 (2001).
- ²¹ K.P. Bohnen, R. Heid, and B. Renker, Phys. Rev. Lett. 86, 5771 (2001).
- ²² T. Yildirim, O. Gulseren, J.W. Lynn, C.M. Brown, T.J. Udovic, Q. Huang, N. Rogado, K.A. Regan, M.A. Hayward, J.S. Slusky, T. He, M.K. Hass, P. Khalifah, K. Inumaru, and R.J. Cava, Phys. Rev. Lett. 87, 37001 (2001).
- ²³ A.Y. Liu, I.I. Mazin, and J. Kortus, Phys. Rev. Lett. 87, 87005 (2001).
- ²⁴ C.W. Chu, T.F. Smith, and W.E. Gardner, Phys. Rev. B 1, 214 (1970).
- ²⁵ H. Kotegawa, K. Ishida, Y. Kitaoka, T. Muranaka, N. Nakagawa, H. Takagiwa, and J. Akimitsu, cond-mat/0201578.

FIG. 1. Lattice parameters a and c for $Mg_{1-x}Al_xB_2$. Experimental data from Ref. [6] (solid circle) and calculated using VCA (open circle).

FIG. 2. Electronic charge density for the MgB_2 (110) plane (top) and the charge density difference between $Mg_{0.5}Al_{0.5}B_2$ and MgB_2 (bottom).

FIG. 3. Electronic band structure and hole Fermi surface for MgB_2 at the calculated lattice constants (see Table I).

FIG. 4. (a) Energy position of the σ -band at E_F and E_A relative to E_F for $Mg_{1-x}Al_xB_2$. In the inset, the hole Fermi surface for $x = 0.25, 0.3$, and 0.35 . (b) Calculated normalized holes FS area, $A(x)=A(0)$ (solid line) and the normalized experimental values (Ref.[8]) of the superconducting critical temperature, $T_c(x)=T_c(0)$ (open circles).

TABLE I. Calculated lattice parameters, cell volume, and density of states at the Fermi level, $N(E_F)$ in states/eV unit cell, for $Mg_{1-x}Al_xB_2$ as a function of Al doping (x).

x	a (Å)	c (Å)	V (Å ³)	$N(E_F)$
0.0	3.083	3.526	29.02	0.72
0.1	3.076	3.486	28.56	0.68
0.2	3.072	3.448	28.18	0.64
0.25	3.070	3.424	27.95	0.60
0.3	3.063	3.403	27.65	0.55
0.35	3.059	3.386	27.44	0.48
0.4	3.055	3.367	27.21	0.43
0.5	3.047	3.338	26.84	0.33
0.6	3.039	3.315	26.51	0.26

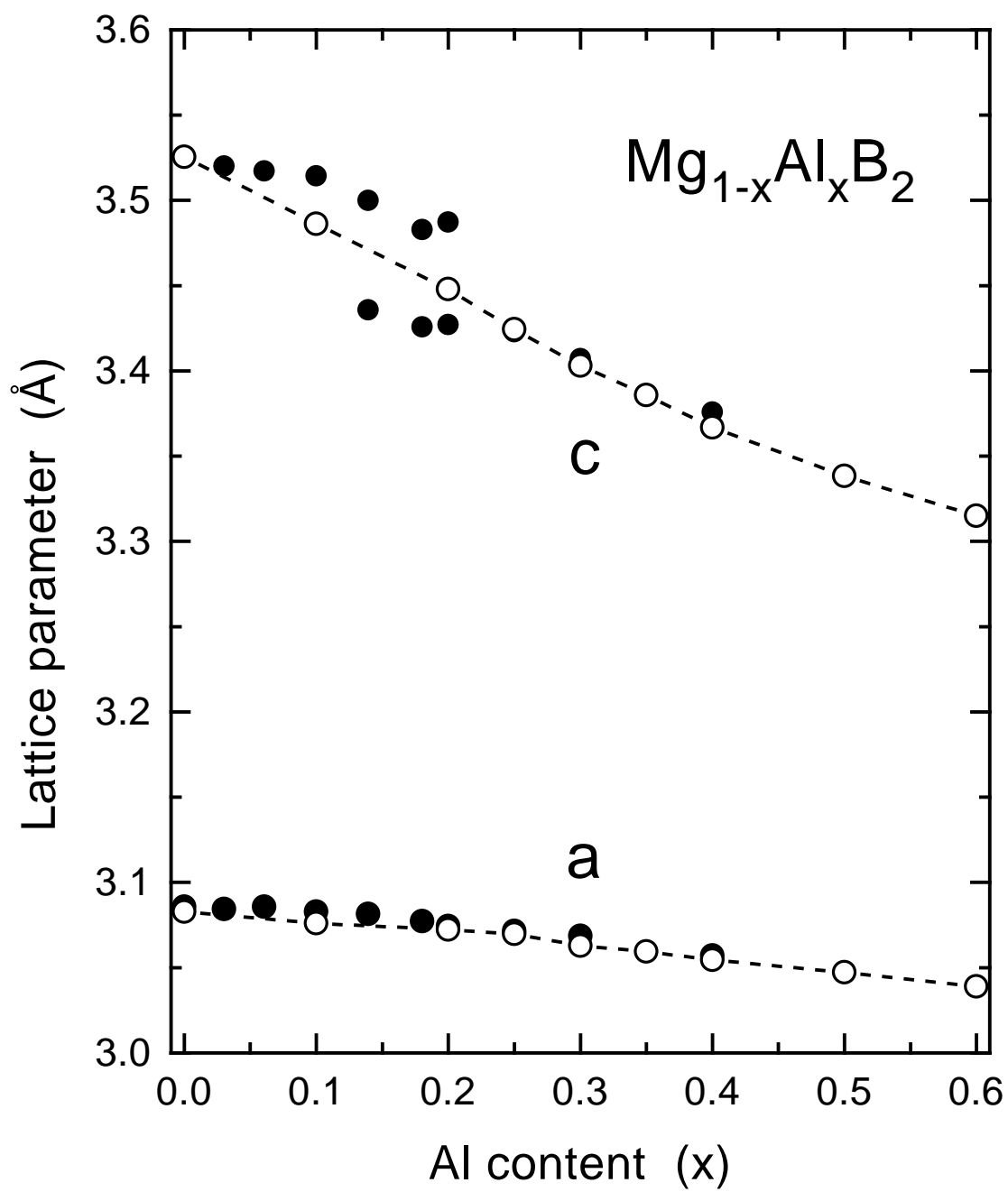


Figure 1. O. de la Peña, et al.

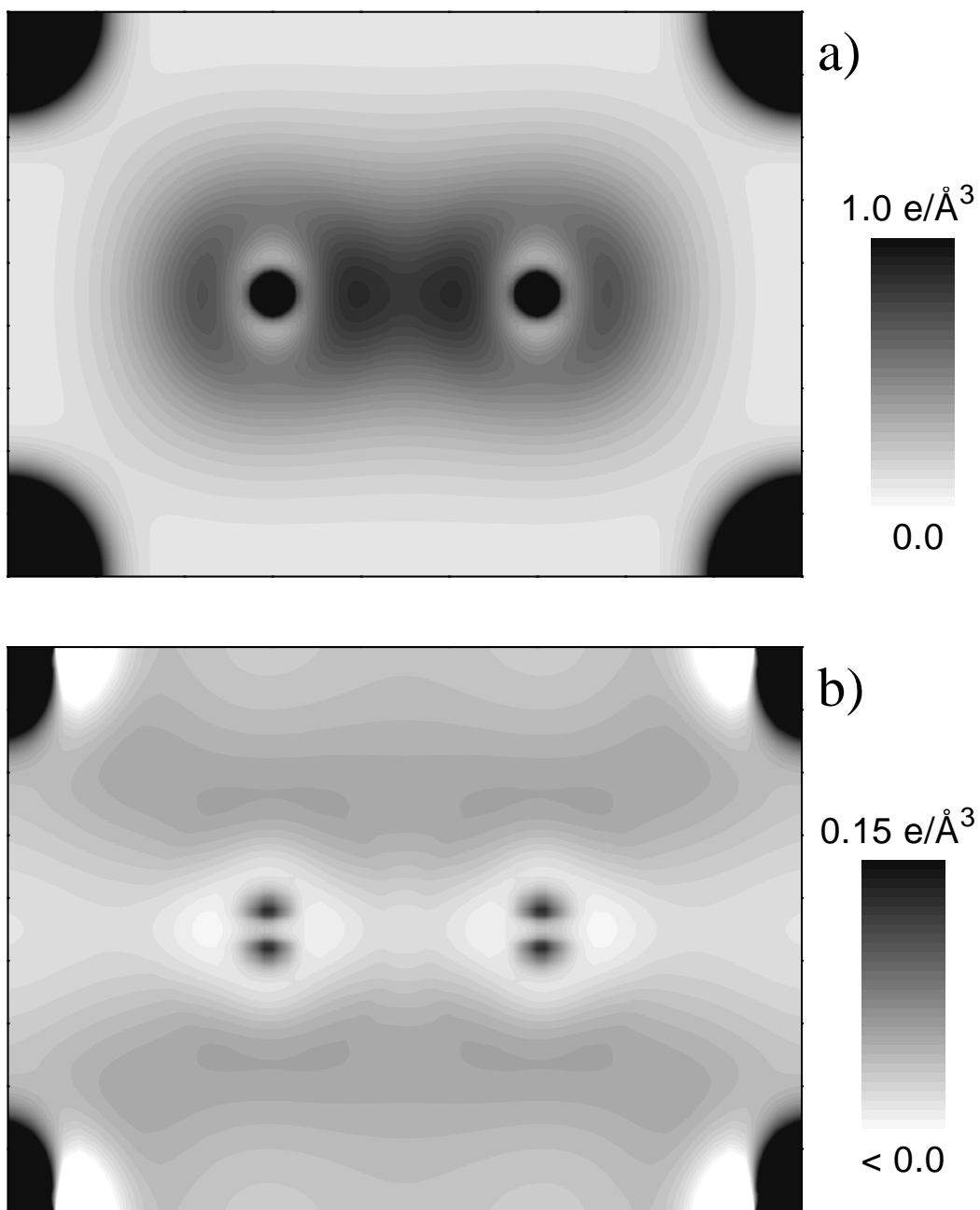


Figure 2. O. de la Peña et al.

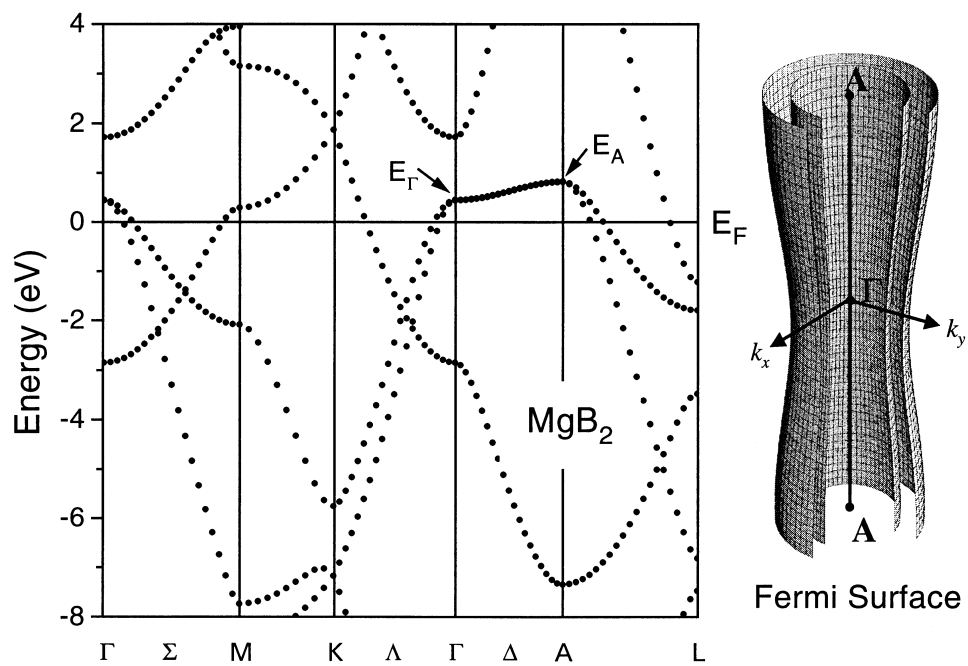


Figure 3. O de la Peña et al.

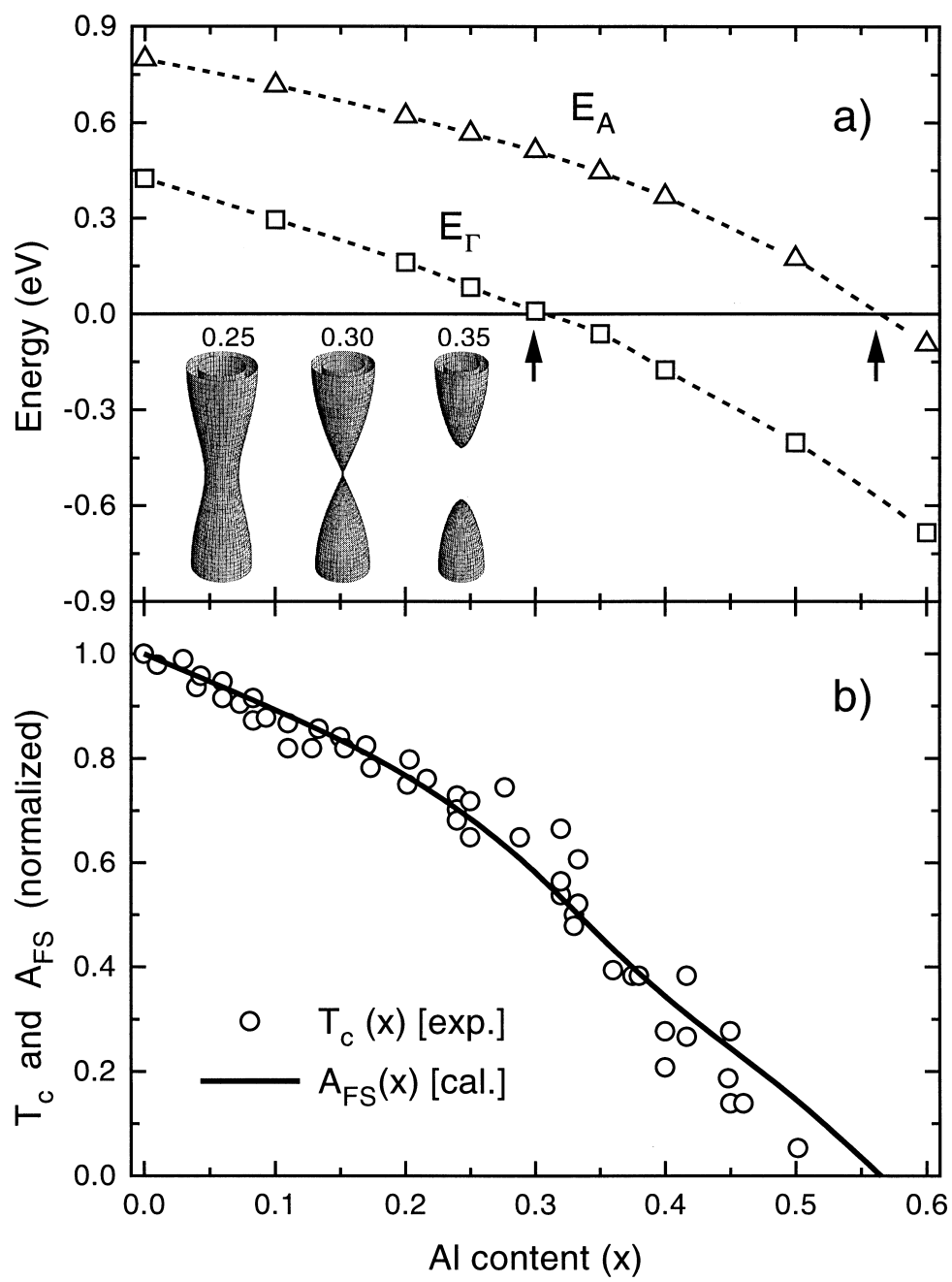


Figure 4. O de la Peña et al.